ACS Catalysis

Research Article

pubs.acs.org/acscatalysis

Quantification of Sophisticated Equilibria in the Reaction Pool and Amplifying Catalytic Cycle of the Soai Reaction

Ilya D. Gridnev*[,†,§] and Andrey Kh. Vorobiev[‡,∥]

[†]Department of Applied Chemistry, Graduate School of Science and Engineering, Tokyo Institute of Technology, Ookayama 2-1-12, Meguro-ku, Tokyo, 185-5550 Japan

[‡]Department of Chemistry, Moscow State University, Vorobievy Gory, Moscow 119991, Russia

Supporting Information

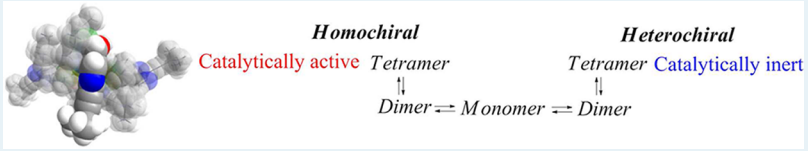

ABSTRACT: The relative abundance of various species in the reaction pool of the Soai autoamplification reaction was estimated by large-scale density functional theory (DFT) computations involving calculations of the thermodynamic parameters in solution. Detailed conformational analysis of the macrocyclic tetrameric species formed by dimerization of the Zn−O−Zn−O square dimers and of their $ZnPr^i_2$ adducts revealed the structural diversification of the homo- and heterochiral species. Homochiral tetramers are exclusively formed in a specific ***brandyglass*** conformation with almost orthogonal pyrimidinyl rings that is virtually unaffected by the formation of a $ZnPr^i_2$ adduct. On the other hand, for heterochiral tetramers the stabilities of ***brandyglass*** and ***layer*** conformations are approximately equal. The three-dimensional (3D) cavity observed in the $ZnPr^i_2$ adduct of the homochiral ***brandyglass*** tetramer forms an ideal chiral pocket for the coordination of the aldehyde followed by perfectly enantioselective alkylation yielding monomeric alcoholate of the same handedness as the tetrameric catalyst. Similar cavity in the heterochiral ***brandyglass*** tetramer is significantly less spacious. Moreover, the cavity practically disappears upon the coordination of $ZnPr^i_2$, hence the heterochiral tetramers are excluded from the flow of catalysis that leads to the realization of Frank's scheme for chiral amplification.

KEYWORDS: *autocatalysis, Soai reaction, Zn alcoholates, DFT computations, solvent effects*

INTRODUCTION

In 1995 Soai et al. discovered that alkylation of certain pyrimidinyl aldehydes with diisopropyl zinc is autocatalytic (Scheme 1) and leads to the amplification of the catalyst chirality.[1] This unique property of the Soai reaction brings the optical purity of the catalyst/product to almost absolute perfection by repeated runs.[2−5] The initial chirality of the sample can be induced by microscopic amounts of chiral inductors.[2−5] Moreover, scalemic samples can be generated from nonchiral precursors via the amplification of stochastic imbalance of the molecules with opposite handedness in racemic samples.[6−13]

Scheme 1. Autoamplifying Soai Reaction

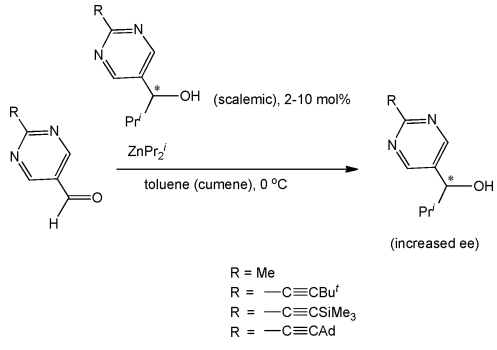

There are two aspects of the mechanism of the Soai reaction. Physicochemical understanding of the amplification and autoamplification phenomena is based on the hypothesis that has been initially formulated by Frank in 1953.[14] Since that time the Frank scheme has been intensively studied theoretically for explaining chiral asymmetry in Nature[15−18] and specifically for the description of the Soai reaction.[19−27] Hence, from the physicochemical point of view there is no lack in possible scenarios that could explain the amplification of chirality in the course of the Soai reaction, as well as the spontaneous break of symmetry in the autocatalytic system. It has been even concluded that numerous reactions of this type are expected to be discovered.[25]

However, this prediction has not come true so far. Moreover, the understanding of purely chemical or structural conditions essential for the practical realization of autoamplification is scarce.[28,29] In other words, we can suggest several kinetic

Received: July 26, 2012
Revised: September 3, 2012
Published: September 5, 2012

   dx.doi.org/10.1021/cs300497h | ACS Catal. 2012, 2, 2137−2149

schemes that would result in the amplification, but we are unable consciously to construct a system that would obey the ideal kinetic scheme, because in a sufficiently sophisticated chemical system the actual behavior of the participating molecules will most probably deviate from our anticipations.

Hence, it is important to look for all possible chemical mechanisms which would explain the specific features of the Soai reaction that would afford a conscious analysis of the crucial factors that are contributing to the successful amplification of chirality. The problem was approached by experimental studies of the reaction pool,[30−33] kinetic measurements,[33−36] and computational analysis.[37−41]

So far, only one possibility for the catalytic cycle of the Soai reaction has been proposed by Schaffiano and Ercolani.[38−41] In this catalytic cycle a dimer catalyst serves as template for the reaction of two molecules of diisopropylzinc with two molecules of aldehyde yielding a tetrameric product that must dissociate to recover the dimeric catalyst and propagate chirality. Possible involvement of a structurally diverse oligomerization in the chiral amplification within the suggested mechanism was discussed.[38] A detailed analysis of the stereochemically different variations of the catalytic cycle[40] and investigation of the reasons for the substrate specificity in the Soai reaction[41] were used to support the soundness of the suggested mechanism.

Schaffiano and Ercolani computed and considered only the species directly involved in the suggested catalytic cycle, whereas the sophisticated equilibria evidently present in the reaction pool containing Zn alcoholates were neglected, implicitly assuming that any species must be kinetically accessible. However, the energy required for the dissociation of the tetrameric product into two molecules of the dimeric catalyst is estimated to be 64.6 kcal mol^{-1} in gas phase and 55.6 kcal mol^{-1} in solution[40] that is inconsistent with a catalytic reaction, since the recovery of the catalyst from the product is virtually impossible if these numbers are true. Although it is claimed that this effect must be leveled on account of the entropy factor, no attempts were made to check the validity of this assumption.

Recently we have analyzed in detail the role of oligomerization in the Soai reaction via a formal kinetic analysis[42] that provided tools for probing various catalytic scenarios via available experimental or computational data. Gas-phase calculations of the possible oligomeric states of the simplified molecules of the catalyst led to the formulation of a conceptually new chemical mechanism involving perfectly enantioselective direct alkyl group transfer in the adduct of the aldehyde and the tetrameric catalyst in a definite conformation.[42]

In this work we report a large-scale computational study in toluene solution of the equilibria in the reaction pool of the Soai reaction using unabridged systems, experimental verification of the computational results, detailed computations of the catalytic cycle involving various orders of the catalyst/product oligomerization, kinetic description of the catalytic cycle, and simulation of the experimental kinetic data.

Two density functional theory (DFT) functionals, B3LYP and M05-2X, were reported to give strikingly different evaluations of the relative stabilities of the species involved in the Soai reaction.[39] We used both of these computational methods to compare their conclusions and assess them to the experimental findings.

RESULTS AND DISCUSSION

Computational Analysis of the Dimeric Resting State in Solution. Experimental studies of the solution behavior of the zinc alcoholates involved in the Soai reaction revealed a complicated system of numerous interconverting species.[30−33] Either solution after reaction completion or solution of alcoholate prepared from the resulting alcohol and diisopropylzinc contains square Zn−O−Zn dimers **A** (Scheme 2) as a

Scheme 2. Structures of Square and Macrocyclic Dimers

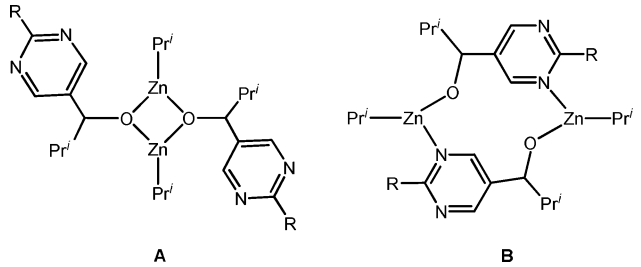

main component.[30−33] On the other hand, the strict substrate specificity required for the autoamplification[43,44] rather implies an involvement of a macrocyclic unit **B** in the formation of a transition state than the Zn−O square structure **A** detected experimentally. It was supposed that square dimers to some degree interconvert in macrocyclic form via dissociation to the monomeric species.[38]

The gas-phase calculations showed that the square dimers **A** are 5−10 kcal mol^{-1} more stable than the macrocycles **B**.[37−41] It has been argued that this situation can be affected by solvent effects, entropy factor, and/or coordination with diisopropylzinc.[38,39] Besides, the 12-membered heterocycle **B** must have numerous conformations for either homo- or heterochiral species that has not been taken in account so far.

Hence we optimized the structures and carried out frequency analyses of the possible dimeric structures in solution (CPCM, toluene) and performed a conformational analysis of the macrocycles **B**.

The dimerization of alcoholate **1** yielding square dimer **2** was computed to be notably exogonic (Scheme 3). If the activation

Scheme 3. Dimerization of Alcoholate 1

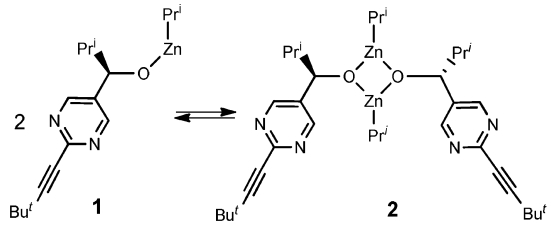

Free energy of dimerization, kcal/mol	ΔE(ZPVE)	ΔG(298.15)	ΔG(273.15)	ΔG(193.15)
B3LYP/6-31G*(cpcm, toluene)	-30.6	-16.0	-17.2	-21.1
M05-2X/6-31G* (cpcm, toluene)	-54.0	-29.2	-30.9	-38.1

barrier for dimerization is neglected, the free energy of dimer dissociation can be estimated as the free energy of interconversion of homo- and heterochiral dimers, taking place via the dissociation to monomer. The latter value has been measured from the DNMR data[45] to be $\Delta G(298)$ = 19.1 kcal mol^{-1}, that is quite close to the absolute value of the computed free energy of dimerization of **1** with the B3LYP functional, whereas the M05-2X evidently overestimates the heat of dimerization (Scheme 3).

The highly exogonic character of dimerization yielding square dimers defines them as building blocks for any higher oligomers.

dx.doi.org/10.1021/cs300497h | ACS Catal. 2012, 2, 2137−2149

Indeed, any "odd" oligomers (trimers, pentamers, etc.) lacking one of the possible Zn−O squares would be disfavored thermodynamically approximately to the same extent as two monomers are less stable than one square dimer.

Table 1 lists the relative energies of various conformations of macrocyclic dimers with respect to the square dimers. We have found that it is convenient to characterize various conformations of a macrocyclic dimer with two angles: ω, an angle between the planes of two pyrimidinyl rings that constitute a macrocycle, and a dihedral angle Zn−O−Zn−O θ, between two Zn−O bonds of the macrocycle (Scheme 4). The search for stable conformations was performed by an energy scan of angle ω that exhibited sharp energy changes when the adjustment of the θ value led to the decrease of the energy.[42]

Table 1. Relative Energies and Gibbs Free Energies (kcal mol^{-1}) of Square and Macrocyclic (Stable Conformations) Dimers Computed in the CPCM (Toluene) Force Field at 6-31G* Level of Theory with Two Different Functionals

		ΔE (ZPVE corrected)		ΔG (298.15)	
configuration	conformation	B3LYP	M05-2X	B3LYP	M05-2X
		Square			
homo		0.0	0.0	0.0	0.0
hetero		−0.1	1.3	0.1	−1.5
		Macrocyclic			
homo	***pancakeae***	9.1	9.5	14.0	8.9
	pancakeaa	10.7	12.0	15.6	10.2
	wineglass	12.7	11.0	15.1	11.0
	waterglass	8.7	6.6	11.1	5.4
hetero	***layer***	6.4	10.1	8.8	7.1
	pancake	11.1	12.3	14.2	9.9
	wineglass	10.6	10.3	13.1	8.9
	waterglass	11.8	8.3	16.2	5.7

Scheme 4. Definition of the Structural Parameters ω and θ for a Zn−O−Zn−N Macrocycle

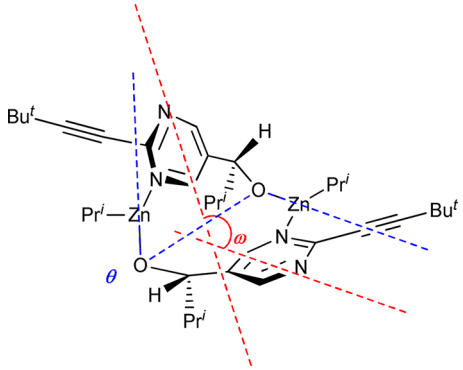

Four stable conformational minima with various combinations of ω and θ were found for either homo- or heterochiral macrocyclic dimers. In either homo- or heterochiral case there are two pairs of conformational minima: one with $\omega > 90°$, and another with $\omega < 90°$. In a homochiral macrocycle four different stable conformations are very close in energy (Table 1, Figure 1). On the other hand, in the heterochiral case the beautiful S_i-symmetric ***layer*** conformation is a definite conformational minimum (Table 1, Figure 2). Notably, the ***layer*** conformation is not a minimum in the homochiral dimer, because one of the Pr^i groups must take an axial position that prevents a coplanar orientation of the pyrimidinyl rings. Hence, a second pancake is the conformational minimum (Figure 1).

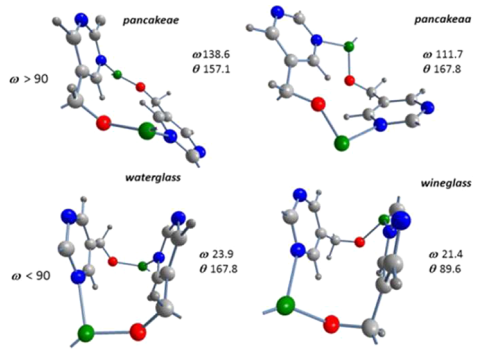

Figure 1. Stable conformations of a homochiral macrocyclic dimer and their characteristic angles. Isopropyl and Bu^t−C≡C− substituents are not shown for clarity.

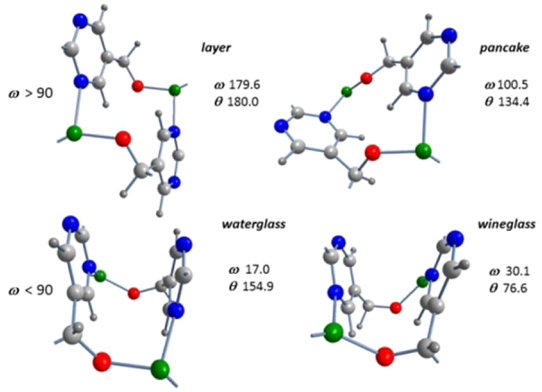

Figure 2. Stable conformations of a heterochiral macrocyclic dimer and their characteristic angles. Isopropyl and Bu^t−C≡C− substituents are not shown for clarity.

Computational Analysis of the Coordination of ZnPr$_2^i$ to Dimers. At least one molecule of ZnPr$_2^i$ should bind to the catalyst to make possible the alkylation of the aldehyde (Scheme 5). Hence, it is important to know how this binding affects the equilibria in the reaction pool of the Soai reaction. We have optimized the structures of the complexes of one or two ZnPr$_2^i$ molecules with various configurations and conformations of homo- and heterochiral dimers (Table 2).

The computations with the B3LYP functional predict mildly endogonic binding of the first ZnPr$_2^i$ molecule at ambient temperature that becomes slightly exogonic at 193 K (Scheme 4). The absence of separate signals for the ZnPr$_2^i$ complexes in the NMR spectra of alcoholates at ambient temperature and their presence at 193 K are in accord with the computational results. M05-2X results predict much stronger binding of dimers with ZnPr$_2^i$ (Table 4). Moreover, unlike B3LYP that attests exclusively for the N-binding, M05-2X suggests that the O-binding can be comparable in strength with the N-binding.

This contradiction between two functionals becomes still more apparent when the coordination of two ZnPr$_2^i$ molecules is considered. Thus, the difference in the relative stability of the ***wineglass*** macrocyclic dimer with two O-bound diisopropylzincs compared to the square dimer with two N-bound ZnPr$_2^i$ molecules estimated with B3LYP and M05-2X achieves 13−20 kcal mol^{-1}. A similar difference has been observed in the gas

dx.doi.org/10.1021/cs300497h | ACS Catal. 2012, 2, 2137−2149

Scheme 5. Coordination of Diisopropylzinc to a Square Dimer 2

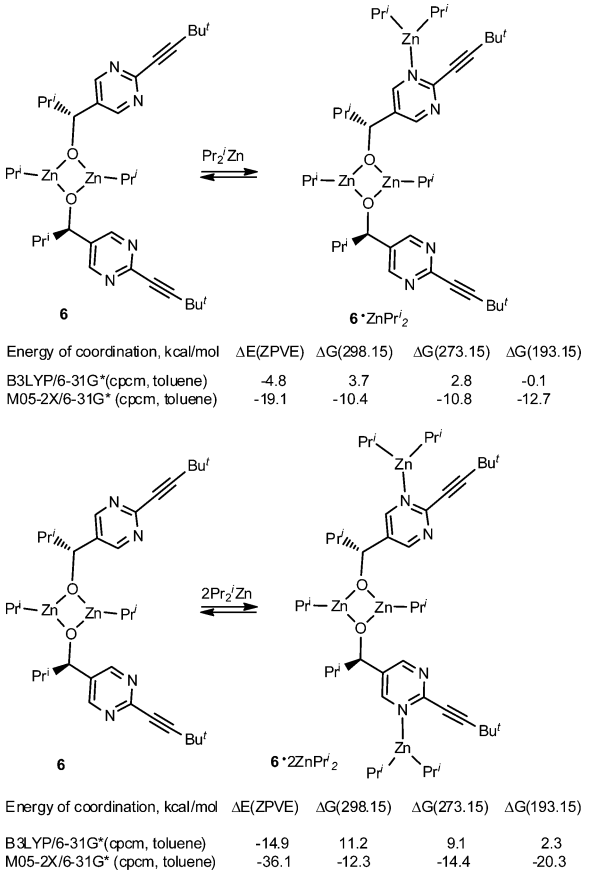

phase calculations with these functionals;[40] hence, this effect is unlikely to be specific for the CPCM solvent model.

The results of this work compared to the available experimental data (vide infra) suggest that this difference reflects some peculiar feature of the M05-2X functional that leads to the significant overestimation of the strength of Zn−N, and especially Zn−O binding. This conclusion has important mechanistic implications, since the catalytic cycle of Schiaffino and Ercolani relies on the M05-2X results, and the ***wineglass*** macrocyclic dimer with two O-bound diisopropylzincs is a key intermediate.[38−41]

Computational Analysis of the Reaction Pool on the Tetramers Level. In the previous section it has been shown that on the dimer level of oligomerization the formation of Zn−O−Zn−O squares prevails over the dimerization resulting in the Zn−O−Zn−N macrocycles. However, the situation is different in the case of tetramers. Further formation of the Zn−O−Zn−O squares encounters significant steric hindrance from the multitude of the isopropyl groups and alkynylpyrimidinyl substituents. As a result, the structures containing only Zn−O−Zn−O binding (Figure 3) are strongly disfavored (Table 3). The association of two square dimers into a macrocyclic tetramer with two pending pyrimidinyl substituents was found to be significantly exothermic in terms of ZPVE corrected electronic energies (Scheme 6). On account of entropy the formation of a tetramer is slightly endogonic at ambient temperature, whereas the ***brandyglass*** tetramer becomes comparable in stability with two square dimers at decreased temperature.

Table 2. Relative Energies and Gibbs Free Energies (kcal mol^{-1}) of $ZnPr^i_2$ Complexes of Square and Macrocyclic (Stable Conformations) Dimers Computed in the CPCM (Toluene) Force Field at 6-31G* Level of Theory with Two Different Functionals

		ΔE(ZPVE corrected)		ΔG (298.15)	
compound	conformation	B3LYP	M05-2X	B3LYP	M05-2X
		Zn1 N-bound Square			
homo		0.0	0.0	0.0	0.0
hetero		−0.3	2.6	0.3	4.0
		Macrocyclic			
homo	***pancakeae***	10.0	11.4	15.6	14.9
	pancakeaa	12.0	13.2	17.5	15.7
	wineglass	14.7	13.7	20.0	17.5
	waterglass	10.3	7.4	13.5	10.0
hetero	***layer***	7.7	12.5	11.6	14.9
	pancake	12.3	14.4	16.9	16.4
	wineglass	12.0	12.1	15.8	16.4
	waterglass	13.3	11.2	17.0	13.5
		Zn1 O-bound Square			
homo		6.3	−1.4	8.5	2.5
macrocyclic					
homo	***wineglass***	10.1	4.9	15.3	6.6
hetero	***wineglass***	10.2	5.2	16.5	10.8
homo	***waterglass***	10.0	4.1	14.5	6.4
		Zn2 N,N-bound Square			
homo		0.0	0.0	0.0	0.0
hetero[a]		0.4	−0.1	1.1	1.2
		Zn2 O,O-bound Macrocyclic			
homo[a]	***wineglass***	14.5	−1.4	21.9	3.8

[a]Relative energies taking homochiral square dimer with N,N-bound two molecules of $ZnPr^i_2$ as a reference.

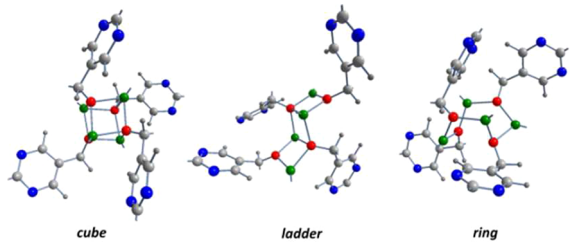

Figure 3. Stable conformations of homochiral Zn−O−Zn−O tetramers. Their relative energies with respect to the homochiral ***brandyglass*** are shown in the Table 3. Isopropyl and Bu^t−C≡C− substituents are not shown for clarity.

This analysis leads to an important conclusion. The macrocyclic units, that are intuitively essential for the autocatalytic Soai reaction, are not seen in dimers, but appear naturally when the dimers tetramerize.

The shape of some stable conformations of the macrocycle in the case of tetramer is strongly affected by the presence of Zn−O−Zn−O squares. Thus, if ***waterglass*** and ***pancakeae*** (***layer*** in the heterochiral case) are very similar with the corresponding conformations in dimers (Figure 1, Figure 2), two other stable conformations are notoriously different. In either homo- or heterochiral case the macrocycle in tetramers instead of ***wineglass*** and ***pancake(aa)*** aquires ***brandyglass*** and ***chair*** conformations, respectively, with almost orthogonal pyrimidinyl rings, but different values of ***θ*** (Figure 4). And, whereas the ***chair*** conformation is evidently destabilized in either homo or

dx.doi.org/10.1021/cs300497h | ACS Catal. 2012, 2, 2137−2149

Table 3. Relative Energies and Gibbs Free Energies (kcal mol^{-1}) of Various Tetramers Computed in the CPCM (Toluene) Force Field at 6-31G* Level of Theory with Two Different Functionals

		ΔE(ZPVE corrected)		ΔG(298.15)	
configuration	conformation	B3LYP	M05-2X	B3LYP	M05-2X
homo	***brandyglass***	0.0	0.0	0.0	0.0
	waterglass	11.4	1.1	15.0	0.4
	pancake	6.2	3.8	7.9	0.9
	chair	9.4	7.5	12.5	5.8
	barrel	7.9	−14.8	15.5	−10.2
	cube	24.4	−2.4	32.3	4.0
	ladder	21.9	9.0	26.6	11.3
	ring	38.8	29.2	44.8	31.5
hetero	***brandyglass***	3.8	3.4	6.3	−2.4
	layer	4.6	6.3	5.6	0.9
	waterglass	6.6	2.7	9.6	3.2
	chair	12.1	−2.3	15.8	−3.6
	barrel	6.7	−17.3	15.7	−13.6

Scheme 6. Formation of Macrocyclic Tetramers from Square Dimers

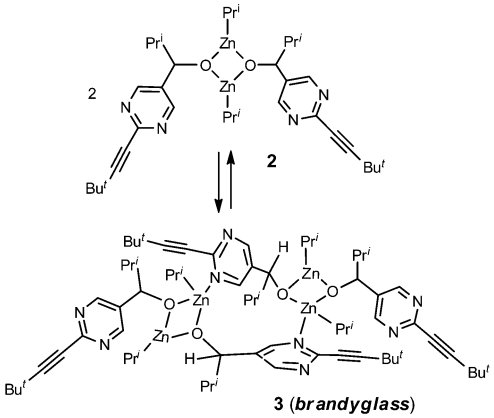

Energy of tetramerization, kcal/mol	ΔE(ZPVE)	ΔG(298.15)	ΔG(273.15)	ΔG(193.15)
B3LYP/6-31G*(cpcm, toluene)	-30.6	5.8	4.1	-1.5
M05-2X/6-31G* (cpcm, toluene)	-42.2	-24.0	-25.4	-29.3

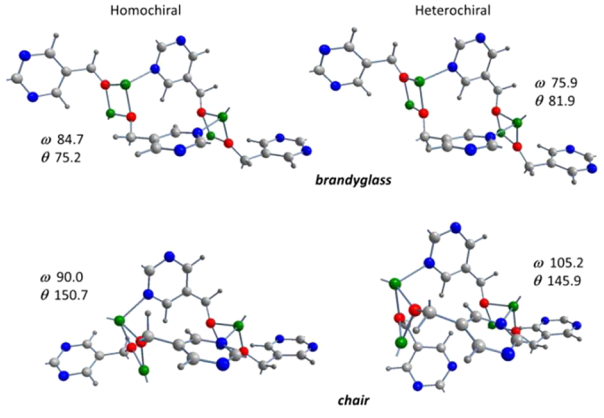

Figure 4. Stable conformations of Zn−N−Zn−O tetramers that are not available at the dimer level. Their relative energies with respect to the homochiral ***brandyglass*** are shown in the Table 3. Isopropyl and Bu^t−C≡C− substituents are not shown for clarity.

Scheme 7. Coordination of $ZnPr^i_2$ to a Homochiral Macrocyclic Tetramer

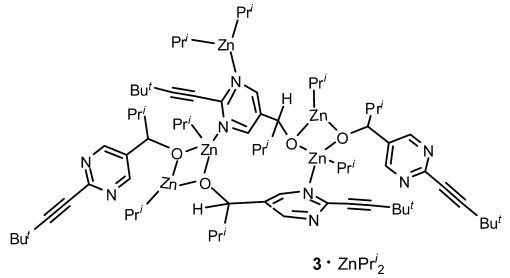

Energy of $ZnPr^i_2$ addition, kcal/mol	ΔE(ZPVE)	ΔG(298.15)	ΔG(273.15)	ΔG(193.15)
B3LYP/6-31G*(cpcm, toluene)	-8.3	6.7	5.5	1.5
M05-2X/6-31G* (cpcm, toluene)	-21.0	-11.4	-12.0	-14.2

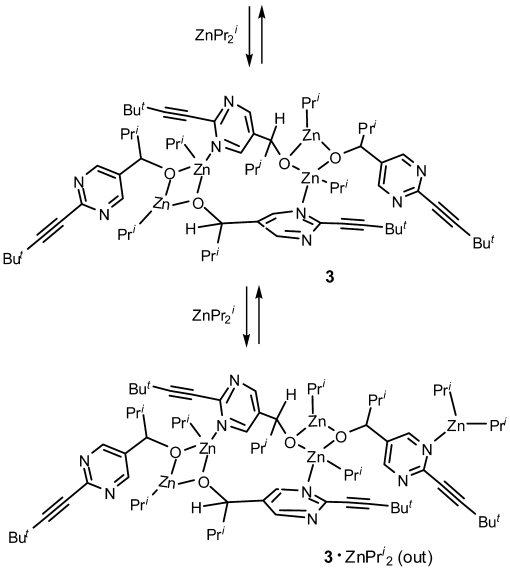

Energy of $ZnPr^i_2$ addition, kcal/mol	ΔE(ZPVE)	ΔG(298.15)	ΔG(273.15)	ΔG(193.15)
B3LYP/6-31G*(cpcm, toluene)	-11.8	6.4	5.2	1.4
M05-2X/6-31G* (cpcm, toluene)	-21.1	-7.1	-12.2	-14.1

heterochiral macrocyclic tetramer, the C_2-symmetrical homochiral ***brandyglass*** is the most stable species among the computed tetramers (Table 3). It has a well-defined cavity formed by the two pyrimidinyl rings that can serve as a chiral pocket for the coordination of the substrate (vide infra).

The shape of the macrocyclic unit in the heterochiral ***brandyglass*** is notably different from the homochiral analogue: the value of ω in the heterochiral species is 75.9° compared to the almost orthogonal pyrimidinyl rings in the homochiral ***brandyglass*** (Figure 4). Importantly, the ***layer*** conformation of the heterochiral macrocyclic tetramer is practically of the same stability as the heterochiral ***brandyglass*** (Table 4), hence the heterochiral tetramers are likely to adopt either of these shapes.

Thus, evident *structural diversification* is observed when the square dimers are producing tetramers: whereas in the homochiral case C_2-symmetrical macrocyclic units bearing widely open cavity are formed, the stable heterochiral tetrameric species have either notably less spacious cavities or, in the case of ***layer***, do not have any cavity at all.

Two functionals give similar estimations of the relative stabilities in most cases indicating the ***brandyglass*** tetramers as the most stable conformation. However, if in the case of B3LYP

dx.doi.org/10.1021/cs300497h | ACS Catal. 2012, 2, 2137−2149

Table 4. Relative Energies and Gibbs Free Energies (kcal mol^{-1}) of Various $ZnPr^i_2$ Complexes of Macrocyclic Tetramers Optimized in the CPCM (Toluene) Force Field at 6-31G* Level of Theory with Two Different Functionals

		ΔE(ZPVE corrected)		ΔG(298.15)		ω, deg.
configuration	conformation	B3LYP	M05-2X	B3LYP	M05-2X	B3LYP
homo	***brandyglass***	0.0	0.0	0.0	0.0	83.8
	brandyglass (out)	−3.5	−3.4	−3.0	−1.9	83.2
	waterglass	10.4	3.3	15.6	12.1	24.1
	pancake	6.8	3.8	6.7	8.2	132.4
	chair	8.4	7.5	11.8	14.6	91.6
	barrel	6.9	−15.3	15.7	−4.1	26.0
						151.6
hetero	***brandyglass***	1.7	1.8	0.4	2.7	66.6
	brandyglass (bad)	3.6	0.3	3.6	2.6	44.1
	brandy (out)	−0.1	0.3	0.7	2.9	73.7
	layer	4.2	2.9	4.3	7.7	176.5
	layer (out)	1.1	*a*	−0.5	*a*	178.3
	water	5.8	1.3	9.3	4.6	26.8
	chair	11.1	6.8	13.3	13.1	105.6
	barrel	5.6	−16.2	14.4	−8.6	93.1
						97.5
						19.2
						149.7

[a]Not computed.

results this conclusion is uniform, M05-2X suggests that homo ***waterglass*** and hetero ***chair*** are comparable in energy with corresponding ***brandyglasses***. This leads to the huge difference in the estimations of the relative stabilities of the homo and heterochiral ***barrels*** that can be formed from macrocyclic tetramers by making two additional Zn−N bonds between the nitrogen atoms of pending pyrimidinyl substituents and the Zn atoms of the Zn−O−Zn−O squares.[37−41] Our results in accord with the computations of Schiaffino and Ercolani[40] suggest that the most stable homochiral ***barrel*** consists from two ***waterglasses***, whereas the most stable heterochiral ***barrel*** is formed from two ***chairs***. With the addition of the mentioned above tendency of M05-2X to overestimate the strength of Zn−N bonds, the calculations result in a huge difference of 25−30 kcal/mol in the relative stabilities of ***barrels*** and ***brandyglasses*** computed with B3LYP and M05-2X (Table 3).

Coordination of $ZnPr^i_2$ to Homo- and Heterochiral Tetramers. As could be expected, the thermodynamic parameters of the $ZnPr^i_2$ addition to a tetramer (Scheme 7) are very similar to those of the same process involving dimers. There are two possible coordination modes in the case of C_2-symmetrical homochiral ***brandyglass*** (Scheme 7) or C_i-symmetrical heterochiral ***layer***. Since the heterochiral ***brandyglass*** is not symmetric, there are totally three possible $ZnPr^i_2$ adducts: two at the macrocyclic unit and one at the pending pyrimidinyl ring.

The homochiral tetramers with other possible conformations of the macrocyclic unit remain relatively unstable upon the $ZnPr^i_2$ coordination (Table 4). On the other hand, in the heterochiral case the $ZnPr^i_2$ adducts of the ***layer*** tetramer with $\omega > 90°$ are comparable in energy with $ZnPr^i_2$ adducts of heterochiral ***brandyglass***.

Although the frequency analysis was not possible at the chosen level of theory for the adducts of two, three, or four molecules of $ZnPr^i_2$ to the tetramers, we have optimized their structures and compared their electronic energies to make sure that such processes do not change the structural features of the stable homo- and heterochiral tetramers.

The shapes of the homochiral ***brandyglass*** and the heterochiral ***layer*** are not notably affected by the coordination of $ZnPr^i_2$ to the macrocyclic unit. On the other hand, the cavity of the heterochiral ***brandyglass*** closes upon the formation of the $ZnPr^i_2$ adducts, approaching in its shape to the ***wineglass*** (Table 4). As a result, neither of the tetrameric heterochiral $ZnPr^i_2$ adducts has a widely open cavity formed by the two pyrimidinyl rings as is seen in the $ZnPr^i_2$ adduct of the homochiral ***brandyglass***, that is, a *structural diversification of homo- and heterochiral* species is observed and becomes more pronounced upon coordination of $ZnPr^i_2$ to tetramers.

The coordination with $ZnPr^i_2$ does not change the situation with the relative stabuilities of ***brandyglasses*** and ***barrels*** dramatically (Table 4). Although the relative stability of the homo- and heterochiral $ZnPr^i_2$ adducts of ***barrels*** computed with M05-2X is notably leveled when the entropy factor is taken into account, it still remains a predominant form in solution even at 298 K.

Consequently, completely different conclusions on the composition of the reaction pool of the Soai reaction on the tetramer level of oligomerization can be made from these two sets of computational data. The B3LYP computations suggest that practically all homochiral tetramers exist in a specific ***brandyglass*** conformation that is not available on the dimer level of oligomerization, and the terminal pyrimidinyl substituents are pending without making additional Zn−N bonds, since it is disfavored, especially with the account of the entropy factor. The formation of ***brandyglass*** shaped tetramers is mildly exogonic at 193 K and mildly endogonic at 273 K (Scheme 6). Hence, the reaction pool must consist of the interconverting square dimers, occasionally formed ***brandyglass*** shaped tetramers and their $ZnPr^i_2$ complexes with equilibrium shifting toward ***brandyglass*** tetramers with decreasing temperature.

Quite oppositely, the M05-2X results suggest that the formation of ***barrels*** is strongly exogonic at any temperature, and the reaction pool must consist essentially from the ***barrels*** only.

dx.doi.org/10.1021/cs300497h | *ACS Catal.* 2012, 2, 2137−2149

We have found a way to resolve this contradiction experimentally. We have computed the ^{1}H NMR spectra of the corresponding homochiral species (Figure 5). It turned out that

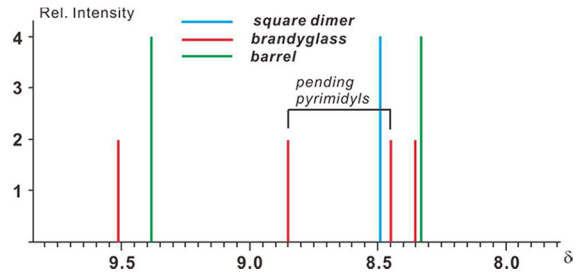

Figure 5. Computed ^{1}H NMR spectra of pyrimidinyl protons in homochiral ***square dimer*** and two homochiral tetramers.

if the pyrimidinyl protons are close to the Zn−O−Zn−O squares, they are notably low-field shifted. As a result, one-third of the homochiral ***brandyglass*** pyrimidinyl protons and half of the homochiral ***barrel*** pyrimidinyl protons are computed to resonate in a very characteristic region of δ 9.0−10.0 (Figure 5). The $ZnPr^i_2$ adducts of both species had approximately the same computed NMR spectra as the noncoordinated species. Since such low-field shifted protons are characteristic for neither of the dimers, the observation of signals in this region can be recognized as the experimental evidence for the formation of tetramers, and measuring the relative intensity of these signals against other pyrimidinyl protons resonating in a normal area of δ 8.0−9.0 can provide the data for a thermodynamic analysis.

An example of the experimental line shape dependence of the pyrimidinyl region of the ^{1}H NMR spectrum of alcoholate is shown in Figure 6. The ratio of the integral intensity of the signals in the region δ 9.0−10.0 to the integral intensity of the signals in the region δ 8.0−9.0 changes from 3: 1 at 193 K to 30: 1 at 253 K, whereas at higher temperatures the species with the low-field shifted signals disappear from the spectra. At higher concentrations the ratio 3: 1 can be maintained at 203 K remaining unchanged upon further decrease of the temperature.[42]

Apparently, these experimental observations are in accord with the B3LYP computational results. Hence, we continued our analysis mainly relying on this functional.

Computational Study of Octamerization. We were interested, whether the further oligomerization would preserve the tendency for the structural diversification of the homo- and heterochiral species; hence, we have optimized structures of several homo- and heterochiral octamers using gas-phase computations at the BLYP/6-31G level of theory (Figure 7).

The superfluity of isopropyl groups in the molecule of an oligomer strictly precludes any deviations from linearity in its structure. Hence, we failed, to construct an octamer consisting exclusively of the ***brandyglass*** units because of the orthogonal orientation of the Zn−O−Zn−O squares in the ***brandyglass***. Nevertheless, if the homochiral macrocyclic ***brandyglass*** and ***wineglass*** units are alternating, beautiful linear octamers **4a** and **4b** are possible (Figure 7). The most stable heterochiral oligomer containing macrocycles with ω < 90° was 14.1 kcal mol^{-1} less stable than **4a**. Noteworthy, all macrocyclic units in **4a** and **4b** have their ω and θ values approximately below 90°. This helps to keep all isopropyls in the molecule apart from the macrocyclic cavities. Hence, a stable indefinite polymer in the homochiral case is likely to have alternating ***brandyglass*** and ***wineglass*** units.

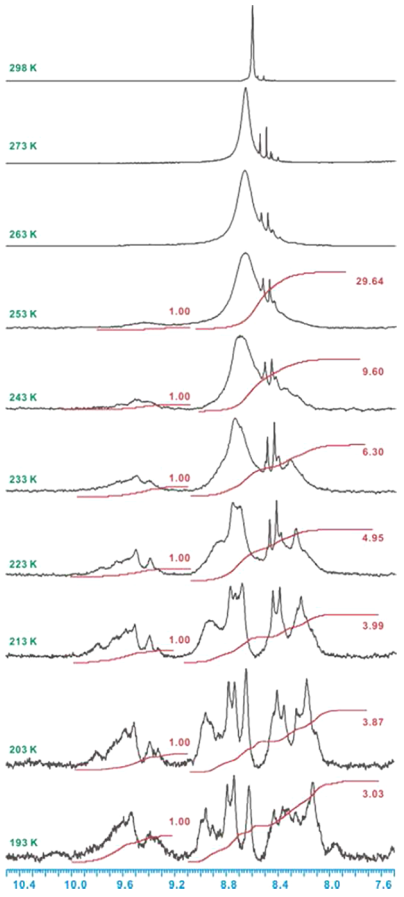

Figure 6. Section plot of the low-field region in the ^{1}H NMR spectrum (400 MHz, toluene/toluene-d_8) of square dimer **2** in equilibrium with ***brandyglass*** tetramer **3** and $ZnPr^i_2$. Alcoholate 0.040 M L^{-1}, excessive $ZnPr^i_2$ 0.040 M L^{-1};.

The situation is opposite for the heterochiral case: the best way to bring all isopropyls apart from the macrocyclic rings is to make an indefinite ***layer*** structure with both ω and θ values close to 180°. This is illustrated with the optimized structure of the octamer **5**, where the terminal macrocyclic units are relaxed into ***pancakes*** (Figure 7). The most stable found homochiral octamer with ω > 90° consisted of ***pancakes*** and was 19.1 kcal mol^{-1} less stable than **5**.

Thus, the structural diversification that has been seen on the tetramer level of oligomerization becomes more prominent upon further polymerization: homochiral oligomers prefer the conformations with ω < 90°, whereas heterochiral oligomers with ω < 90° are strongly disfavored. And vice versa, the structures with ω > 90° are stable in the heterochiral case, while homochiral oligomers with ω > 90° are destabilized.

This means that homo and heterochiral higher oligomers must have different properties, for example, solubility, and carrying out the reaction in some particular solvent may result in the precipitation of heterochiral oligomers, leaving in solution only homochiral species, that would provide additional source of the amplification of chirality.

Experimental Estimation of the Thermodynamic Parameters of Tetramerization. To have an idea of the appearance of the low temperature spectrum of the equilibrium mixture of alcoholates without coordinated $ZnPr^i_2$, we have measured the ^{1}H NMR of a sample prepared from the corresponding homochiral alcohol **6** with the deficiency of

dx.doi.org/10.1021/cs300497h | ACS Catal. 2012, 2, 2137−2149

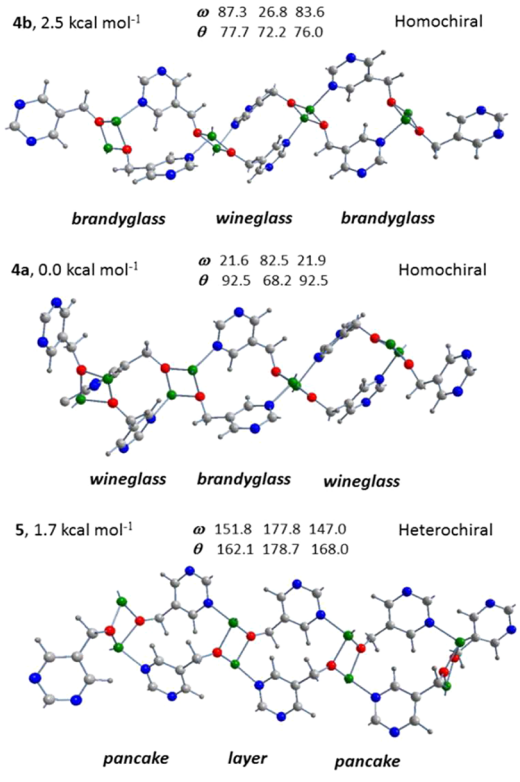

Figure 7. Structures of the most stable homo- and heterochiral octamers optimized on the BLYP/6-31G level of theory. Isopropyl and Bu^t–C≡C– substituents are not shown for clarity.

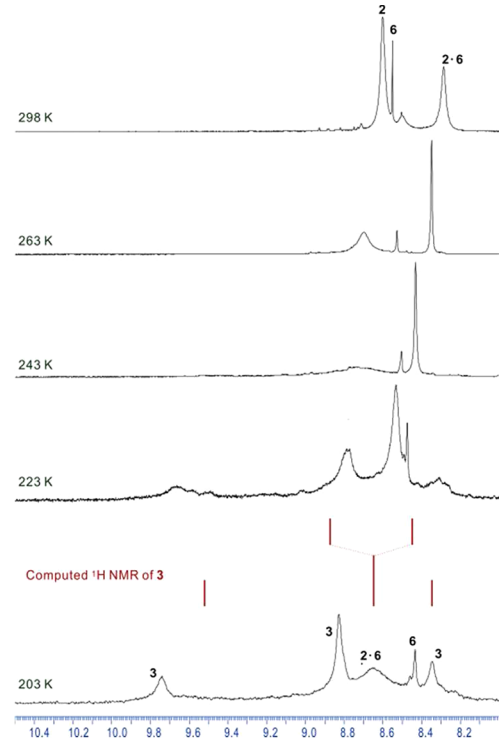

Figure 8. Section plots of the low-field region in the ^{1}H NMR spectrum (400 MHz, toluene/toluene-d$_8$) of square dimer **2** in equilibrium with ***brandyglass*** tetramer **3** and alcohol **6**: alcoholate 0.015 M L^{-1}, excessive alcohol **6** 0.013 M L^{-1}.

diisopropylzinc, so the sample contained besides the alcoholate **1** (equiliblium mixture of oligomers) free alcohol **6** and its complex with alcoholate that according to the 2D ^{1}H-^{1}H EXSY spectrum were in a slow exchange with each other at ambient temperature (Scheme 8). As can be seen from Figure 8, the spectrum of alcoholate at 203 K consists of three signals at δ 9.74, 8.85, and 8.34 in a ratio 1:2:1 that qualitatively corresponds to the computed spectrum of the ***brandyglass*** tetramer taking into account that the nonequivalence of the two protons from each of the pending pyrimidinyl rings seen in the computed spectrum is actually removed in the measured spectrum because of the fast conformational rotation.

Scheme 8. Reaction of the Chiral Alcohol 2b with Deficiency of Diisopropylzinc

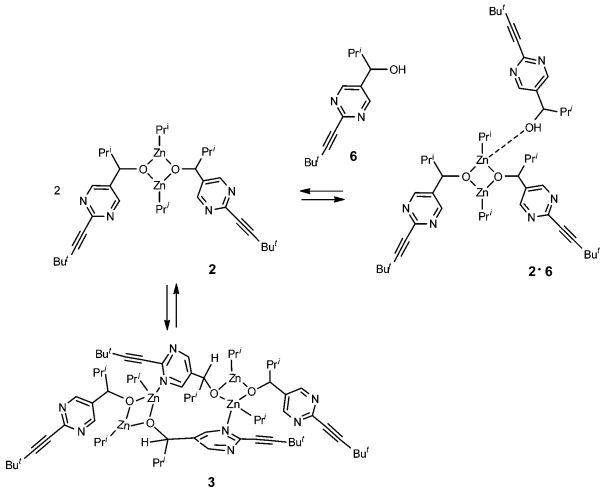

The temperature dependence of the ratio of the integral intensity of the low-field signal of **3** to the integral intensity of the signals in the region δ 8.0–9.0 went through a maximum at 203 K, and decreased at lower temperatures in this sample. We attribute this to further oligomerization: in the previous section it has been shown that two ***brandyglasses*** cannot exist in the neighboring positions; hence, in a hexamer only one of two macrocyclic units would have low-field shifted protons. Indeed, the computed spectrum of the homochiral hexamer had two signals in the lower field region (δ 9.74, 8.85) and 10 signals between δ 8.0 and δ 9.0. Thus, the experimetally measured values of ξ - the ratio of the integral intensities of the low-field (δ > 9.0) and high-field (δ > 9.0) pyrimidinyl protons, can be used for the evaluation of the thermodynamic characteristics of oligomerization. We have considered two equilibria:

$$2D \rightleftarrows T, \quad K_T$$

$$T + D \rightleftarrows H, \quad K_H$$

The concentrations of each component and values of ξ were computed with the account of stoichiometry from the given values of enthalpy and entropy for each equilibrium. The value $(\xi_{calc} - \xi_{exp})/\xi_{exp}$ was minimized by variation of enthalpies and entropies via a nonlinear regression approach with the program NL2SOL.[46] The best-fit curve for the temperature dependence of ξ is shown in Figure 9 together with the thermodynamic parameters used for its calculation. Comparing the experimentally found values of Gibbs free energies of tetramerization

dx.doi.org/10.1021/cs300497h | ACS Catal. 2012, 2, 2137–2149

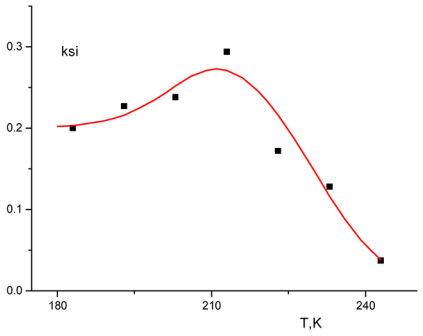

K_T: ΔH = –20.3±3.3 kcal mol^{-1}; ΔS = –78±14 cal mol^{-1} K^{-1}

K_H: ΔH = –27.8±18.4 kcal mol^{-1}; ΔS = –121±90 kcal mol^{-1}

Figure 9. Experimental values of ξ at various temperatures and best-fit computed temperature dependence of ξ calculated with the thermodynamic parameters shown below.

$$\Delta G(298) = 2.9 \pm 4.2 \text{ kcal mol}^{-1};$$
$$\Delta G(193) = -5.2 \pm 3.3 \text{ kcal mol}^{-1}$$

to the computed values shown in Scheme 6, one can find a nice qualitative agreement between experiment and computations with the B3LYP functional.

As mentioned above, in the presence of excessive diisopropylzinc the temperature dependence of ξ is different displaying the monotonic achievement of the value 1/3 that is characteristic for ***brandyglass*** tetramers. Hence, the coordination of $ZnPr^i_2$ locks the active sites of the alcoholate that reduces the order of its association. As a result, in the presence of the excessive diisopropylzinc no adducts higher than tetramers are observed in the NMR. Assuming that the thermodynamic parameters of the $ZnPr^i_2$ binding are the same for all adducts, we have estimated their values from the NMR data via nonlinear regression. Treatment of 41 experimental values of ξ afforded the values

$$\Delta H = -10.7 \pm 1.5 \text{ kcal mol}^{-1};$$
$$\Delta S = -40 \pm 7 \text{ cal mol}^{-1} \text{ K}^{-1}$$

The obtained Gibbs free energies

$$\Delta G(298) = 1.2 \text{ kcal mol}^{-1};$$
$$\Delta G(193) = -5.2 \text{ kcal mol}^{-1}$$

are in a reasonable agreement with the values computed with the B3LYP functional (Scheme 7).

Thus, from our combined computational and experimental NMR study we concluded that the reaction pool of the Soai reaction consists of square dimers in equilibrium with small concentrations of ***brandyglass*** tetramers and their $ZnPr^i_2$ adducts in the case of enantiopure samples. In scalemic samples the approximate statistical distribution between homo- and heterochiral species is maintained on any level of oligomerization, but a structural diversification takes place: homochiral tetramers are formed in the ***brandyglass*** conformation with an open cavity, whereas heterochiral oligomers are approximately equally distributed between closed ***brandyglasses*** and ***layers***.

Computation of the Catalytic Cycle with the Homochiral Brandyglass Tetramer as a Catalyst. We reasoned that the unique shape and accessibility of the three-dimensional (3D) cavity in the homochiral tetramer might be the origin of its high catalytic activity. Indeed, a substrate molecule has a suitable shape complementarity to the cavity of **3**·$ZnPr^i_2$ (Figure 10). The electrophilicity of the substrate aldehyde group is increased upon

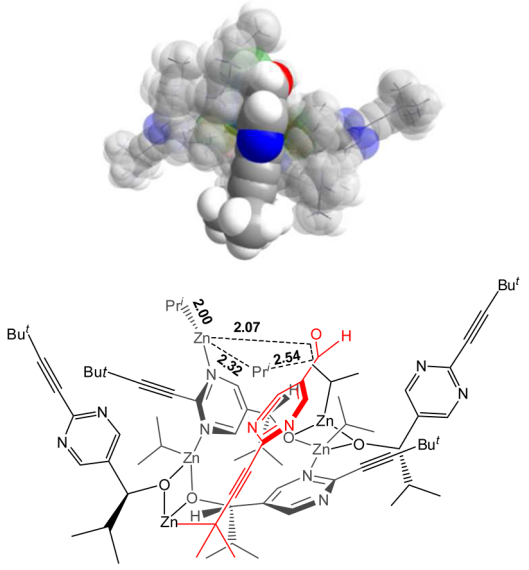

Figure 10. Transition state for the direct transfer of the isopropyl group from the N-bound $ZnPr^i_2$ computed for the alkylation of aldehyde with the catalyst **3** (B3LYP/6-31G (CPCM, toluene)). The importance of the specifically shaped substrate accurately fitting to the cavity is illustrated on the space-filling model.

coordination to Zn, whereas the Bu^t–C≡C– substituent of the pyrimidyl ring serves as a structural anchor leading to a well-defined substrate orientation. This specific coordination discriminates between the prochiral planes of the aldehyde, since an approach of the oxygen atom to the Zn atom is only possible with one of the prochiral planes. A transition state (**TS1**) for the direct isopropyl group transfer from **3**·$ZnPr^i_2$ was located (Figure 10), leading to the formation of the product with the same handedness as the tetrameric catalyst. A catalytic cycle involving the enantioselective direct alkyl transfer is shown in the Figure 11. It begins from the coordination of diisopropylzinc to the catalyst that is followed by the coordination of aldehyde. After the alkyl transfer the catalyst is recovered dissociating a monomeric alcoholate that amplifies the chiral pool of the reaction.

Unfortunately, the frequency analysis was not available for the unabridged molecules larger than the $ZnPr^i_2$ adduct of the tetramer at the B3LYP/6-31G* (CPCM, toluene) level of theory. Hence, we computed the catalytic cycle at the B3LYP/6-31G (CPCM, toluene) and B3LYP/6-31G* (gas phase) levels of theory that gave similar results (Figure 11).

Simulation of Kinetics of the Computed Catalytic Cycle. The following assumptions derived from the computed/measured equilibrium constants at various temperatures were used for building the kinetic model:

(1) The reaction product exists in solution mainly as the dimer.

(2) The concentrations of monomers, tetramers, or higher oligomers are negligible.

(3) Catalytic activity is displayed by the homochiral tetramers.

(4) The strength of the $ZnPr^i_2$ association to the oligomers varies considerably with the temperature and concentrations of the reagents. This association strongly affects the equilibrium

dx.doi.org/10.1021/cs300497h | ACS Catal. 2012, 2, 2137–2149

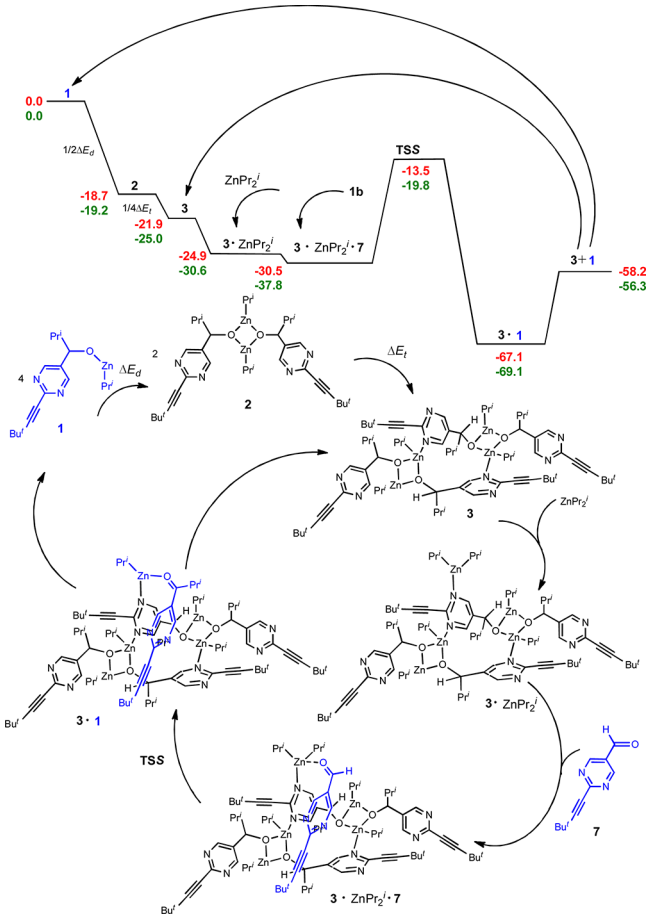

Figure 11. Catalytic cycle for the alkylation of aldehyde **7** with the catalyst **3** computed on the B3LYP/6-31G/CPCM(toluene) level of theory (red numbers) or B3LYP/6-31G* (green numbers). The numbers correspond to the relative entalpies in kcal mol^{-1}.

between dimers and tetramers. Hence, these equilibria were considered in an explicit form.

(5) The aldehyde binding leading to the reactive adduct is weak.

To simplify the quantitative description, we have additionally used the following assumptions:

(6) Dimers and tetramers bind only one molecule of diisopropylzinc. The binding constants of $ZnPr^i_2$ with dimers and tetramers were considered to be the same.

(7) Homo and hetero alcoholate dimers are formed in a statistical proportion.

With these assumptions the kinetic equations describing the accumulation of the reaction products and evolution of enantiomeric excess adopt the following form (see Supporting Information):

$$\frac{dC}{dt} = (C_0 + A_0 - C)\cdot Zn\cdot[4k_r D^2((1+ee)^4 - (1-ee)^4) + 2k_0]$$

$$\frac{dee}{dt} = \frac{(C_0 + A_0 - C)\cdot Zn\cdot D}{1 + K_{DZn}Zn}\left[2k_r\cdot((1+ee)^4(1-ee) - (1-ee)^4(1+ee)) - \frac{k_0\cdot ee}{K_D^2}\right] \quad (1)$$

where C_0 and A_0 are the starting concentrations of alcoholate and aldehyde, concentrations of nonbound dimers D and nonbound diisopropylzinc Zn are determined by the following equations:

$$Zn_\Sigma = Zn_0 - C + C_0$$

$$D = (\sqrt{(1/K_{DZn} + Zn_\Sigma - C/2)^2 + 2C/K_{DZn}} - 1/K_{DZn} - Zn_\Sigma + C/2)/2$$

$$Zn = Zn_\Sigma/(1 + K_{DZn}D)$$

and the expression for the kinetic constant contains the equilibrium constants:

$$k_r = \frac{k_1 K_A K_{TZn} K_T}{2^6} \quad (2)$$

where k_1 is the rate constant $k_r = k_b T/h \exp[-\Delta H_{ts}/k_b T + \Delta S_{ts}/k_b]$; K_T is the equilibrium constant between dimer and tetramer species; K_{TZn} and K_{DZn} are the equilibrium constants for diisopropylzinc attachment to tetramer and dimer species, respectively; K_A is the equilibrium constant for substrate attachment to tetramer-diisopropylzinc complex.

As follows from the eq 2, the temperature dependence of the kinetic constant k_r is determined not only by the properties of the transition state, but also by the thermodynamic parameters of the formation of the tetramer from the dimers, addition of $ZnPr^i_2$ and aldehyde:

$$k_r = \frac{k_b T}{h}\exp\left[-\frac{\Delta H_r}{k_b T} + \frac{\Delta S_r}{k_b}\right]$$

$$\Delta H_r = \Delta H_{ts} + \Delta H_A + \Delta H_{TZn} + \Delta H_T$$

$$\Delta S_r = \Delta S_{ts} + \Delta S_A + \Delta S_{TZn} + \Delta S_T \quad (3)$$

The equation for the rate constant does not contain the thermodynamic parameters for the dissociation of monomer from the pentamer **3**·**1** and for the dimerization of **1** to **2** because of the applied assumption that all equilibria between various alcoholates are fast and rapidly established.

Kinetic curves obtained by numerical solution of the eqs 1 are shown in the Figure 12. A qualitative agreement with the

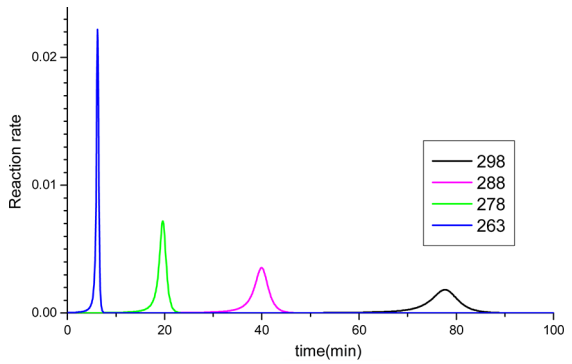

Figure 12. Kinetic curves calculated with (1) using the values of ΔH_r and ΔS_r to fit the experimental kinetic curves.[33] The following initial parameters were used: ee_0 = 1.0; A_0= 0.015 M; $C_0 = A_0/100$.

experimental curves[33] was obtained with the values $\Delta H_r = -12.0$ kcal mol^{-1}, $\Delta S_r = -63$ cal mol^{-1} K^{-1}. Estimation of the kinetic constant components using the eqs 3 and the data obtained by the computation of the catalytic cycle (Table 5) give the following values: $\Delta H_r = -14.6$ kcal mol^{-1}, $\Delta S_r = -183$ cal mol^{-1} K^{-1}(B3LYP/6-31G*(gas phase).

Apparently, the computations can reasonably well reproduce the activation enthalpy taking into account inaccuracies caused

dx.doi.org/10.1021/cs300497h | ACS Catal. 2012, 2, 2137−2149

Table 5. Computed and Experimentally Found Values of the Thermodynamic Parameters for the Important Stages of the Catalytic Cycle

	ΔH, kcal mol^{-1}				ΔS, cal mol^{-1} K^{-1}			
	B3LYP/6-31G* (gas phase)	B3LYP/6-31G (cpcm, toluene)	M052X/6-31G (cpcm, toluene)	experimental[a]	B3LYP/6-31G* (gas phase)	B3LYP/6-31G (cpcm, toluene)	M052X/6-31G (cpcm, toluene)	experimental[a]
tetramerization, 2D ⇄ T K_T	−21.9	−12.3	−42.8	−20.3 ± 3.3	−74	−22	−79	−78 ± 14
Zn addition to tetramer, T + $ZnPr^i_2$ ⇄ T_{Zn} K_{TZn}	−8.4	−5.6	−15.8	−10.7 ± 1.5	−54	−40	−38	−40 ± 7
addition of aldehyde T_{Zn} + Al ⇄ T_{ZnAl} K_A	−1.9	−1.1	−14.4		−43	−54	−53	
alkylation	17.6	17.0	11.1		−12	−9	−18	

[a]This work, vide supra.

by the accepted assumptions, and so forth. On the other hand, the computed value of the activation entropy is significantly more negative than the value satisfactorily describing the experiment. Presumably, the main source of this error is the well-known major computational challenge for the accurate calculation of entropies, for which no universal resolution is known so far.[47−49] One should also take into account that the experimental data were obtained for a slightly different substrate.[33]

Dividing eqs 1 one into another, one can get a convenient expression for the calculation of the resulting *ee* values:

$$\frac{d\boldsymbol{ee}}{dC} = \frac{\boldsymbol{D}\cdot[2((1+\boldsymbol{ee})^4(1-\boldsymbol{ee}) - (1-\boldsymbol{ee})^4(1+\boldsymbol{ee})) - \boldsymbol{w}_0\boldsymbol{ee}/\boldsymbol{K}_D^2]}{(1+\boldsymbol{K}_{DZn}\boldsymbol{Zn})\cdot[4\boldsymbol{D}^2((1+\boldsymbol{ee})^4 - (1-\boldsymbol{ee})^4) + 2\boldsymbol{w}_0]} \quad (4)$$

where $\boldsymbol{w}_0 = \boldsymbol{k}_0/\boldsymbol{k}_r$.

Equation 4 does not contain the components of the kinetic constant $\boldsymbol{k}_r$, $\Delta\boldsymbol{H}_r$, $\Delta\boldsymbol{S}_r$, if the rate of the noncatalytic alkylation is negligible.

From Supporting Information, Table S1 one can see that the experimental regularities of the accumulation of *ee* during the reaction are well reproduced in terms of the accepted model. However, it should be taken into account that these regularities are not mechanism specific, that is, they can be the same for various amplification mechanisms.[42]

Influence of a Background Reaction. The main source of amplification of chirality within the suggested mechanism is the *structural diversification* of the homo- and heterochiral species during reversible formation of macrocyclic tetramers from the square dimers. In other words, the tetramerization of homo- and heterochiral species occurs with comparable effectiveness, but the structures of homo- and heterochiral tetramers are different, so that only homochiral species can effectuate the catalysis. The suggested mechanism of the direct alkyl transfer is perfectly enantioselective, that is, no *R* enantiomer can be produced by the S_4 catalyst. However, a background noncatalytic reaction may interfere and affect the amplification process.

The influence of a background nonselective reaction on the amplification was analyzed by numerical simulation as shown in the Figure 13. Irrespectively of the relative rate of the background reaction, the final enantiomeric excess reaches the value 1.0, but the time required for that increases with the increasing relative rate of the background reaction.

Hence, although in an ideal case the background reaction does not spoil the amplification, the elongation of the reaction time required for its realization may result in intervention of various disturbing factors like precipitation or oxidation of the catalyst, and so forth. As a result, the background reaction may be one of the reasons for an not perfect amplification in the Soai reaction.

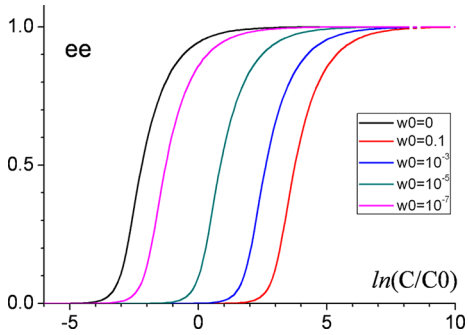

Figure 13. Dependence of the enantiomeric excess vs conversion at different relative rates of a noncatalytic reaction computed using the eq 4.

CONCLUSIONS

A combined computational and experimental study of the reaction pool resulted in the formulation of a new chemical mechanism for the autoamplifying Soai reaction. The formation of tetramers from Zn−O−Zn−O dimers creates the conditions for amplification of chirality through enantioselective direct alkylation catalyzed by a homochiral macrocyclic Zn−N−Zn−O tetramer that aquires specific ***brandyglass*** conformation with orthogonal pyrimidinyl rings that is preserved upon coordination of $ZnPr^i_2$. The same conformation is not achieved either in the heterochiral tetramer itself or in its $ZnPr^i_2$ adduct that excludes heterochiral tetramers from the flux of catalysis.

Computations of the several individual stages of the catalytic cycle gave the results that stand in reasonable accordance with the experimental data. Detailed computation of the catalytic cycle and simulation of its kinetics revealed no evident contradictions to the known experimental data.

At the very least, the suggested mechanism demonstrates one of the possible chemical scenarios that can result in the amplification of chirality. Hence, it gives important information for the general understanding of this phenomenon from the chemical point of view. Since a lot of crucial factors contribute to the realization of this mechanism, it would not be enough to synthesize a catalyst with the structure resembling the ***brandyglass*** conformation of the homochiral tetramer to mimic the amplification of chirality observed in the Soai reaction. Numerous requirements for reversibility of different stages, relative abundance of homo- and heterochiral species, and so forth must come together to realize the amplification of chirality.

These considerations explain well the strict substrate specificity that is well-known for the Soai reaction. Furthermore, they demonstrate the prospects of further studies in modeling the rare phenomenon of autoamplification, since they increase

dx.doi.org/10.1021/cs300497h | ACS Catal. 2012, 2, 2137−2149

our knowledge of the regularities of sophisticated chemical processes.

EXPERIMENTAL SECTION

NMR spectra were recorded on the JEOL ESA-400 and JEOL ESA-600 spectrometers. Aldehyde **7** was prepared according to the known procedures.[9,43] Diisopropylzinc was purchased from Aldrich as 1.0 M solution in toluene. All operations were performed under an atmosphere of dry argon using conventional Schlenk techniques.

Computations were carried out using the hybrid Becke functional (B3)[50,51] for electron exchange and the correlation functional of Lee, Yang, and Parr (LYP),[52] or M05-2X functional[53] as implemented in the GAUSSIAN 09 software package.[54] All atoms were modeled at the 6-31G or 6-31G(d) level of theory.[55−59] Starting geometries for the transition state search were located either by QST2 or QST3 procedures, or by the guess based on the structure of the previously found TS. The transition states were subsequently fully optimized as saddle points of first order, employing the Berny algorithm.[60] Frequency calculations were carried out to confirm the nature of the stationary points, yielding zero imaginary frequencies for all minima and one imaginary frequency for all transition states, which represented the vector for the C−C bond formation. The solvent influence has been accounted for by carrying out optimizations in the CPCM force field.[61,62]

ASSOCIATED CONTENT

Supporting Information

Derivation of the eqs 1−4. Cartesian coordinates and computed energies of all optimized conformational minima and transition states. This material is available free of charge via the Internet at http://pubs.acs.org.

AUTHOR INFORMATION

Corresponding Author

*E-mail: igridnev@m.tohoku.ac.jp.

Present Address

[§]Department of Chemistry, Graduate School of Science, Tohoku University, Aramaki 3-6, Aoba-ku, Sendai, 980-8578, Japan.

Funding

This work was supported by Chemistry GCOE Program of Tokyo Institute of Technology.

Notes

The authors declare no competing financial interest.

[∥]E-mail: a.kh.vorobiev@gmail.com.

ACKNOWLEDGMENTS

Computations reported in this paper were carried out on the Tsubame supercomputer at Tokyo Institute of Technology.

REFERENCES

(1) Soai, K.; Shibata, T.; Morioka, H.; Shoji, K. *Nature* **1995**, *378*, 767.
(2) Soai, K.; Shibata, T.; Sato, I. *Acc. Chem. Res.* **2000**, *33*, 382.
(3) Soai, K.; Kawasaki, T. *Chirality* **2006**, *18*, 469.
(4) Soai, K.; Kawasaki, T. *Top. Curr. Chem.* **2008**, *271−274*, 1.
(5) Kawasaki, T.; Soai, K. *Bull. Chem. Soc. Jpn.* **2011**, *84*, 879.
(6) Soai, K.; Shibata, T.; Kowata, Y. JP-Kokai 9-268179, 1997.
(7) Singleton, D. A.; Vo, L. K. *J. Am. Chem. Soc.* **2002**, *124*, 10010.
(8) Soai, K.; Sato, I.; Shibata, T.; Komiya, S.; Hayashi, M.; Matsueda, Y.; Imamura, H.; Hayase, T.; Morioka, H.; Tabira, H.; Yamamoto, J.; Kowata, Y. *Tetrahedron: Asymmetry* **2003**, *14*, 185.
(9) Gridnev, I. D.; Serafimov, J. M.; Quiney, H.; Brown, J. M. *Org. Biomol. Chem.* **2003**, *1*, 3811.
(10) (e) Singleton, D. A.; Vo, L. K. *Org. Lett.* **2003**, *5*, 4337. (f) Kawasaki, T.; Suzuki, K.; Shimizu, M.; Ishikawa, K.; Soai, K. *Chirality* **2006**, *18*, 479.
(11) Barabas, B.; Caglioti, L.; Zucchi, C.; Maioli, M.; Gal, E.; Micskei, K.; Palyi, G. *J. Phys. Chem. B* **2007**, *111*, 11506.
(12) Micskei, K.; Rabai, G.; Gal, E.; Caglioti, L.; Palyi, G. *J. Phys. Chem. B* **2008**, *112*, 9196.
(13) Suzuki, K.; Hatase, K.; Nishiyama, D.; Kawasaki, T.; Soai, K. *J. Syst. Chem.* **2010**, *1*, 5.
(14) Frank, F. C. *Biochim. Biophys. Acta* **1953**, *11*, 459.
(15) Avetisov, V.; Goldanskii, V. I. *Proc. Natl. Acad. Sci. U.S.A.* **1996**, *93*, 11435.
(16) Goldanskii, V. I.; Kuzmin, V. V. *Z. Phys. Chem. (Leipzig)* **1988**, *269*, 216.
(17) Mislow, K. *Collect. Czech. Chem. Commun.* **2003**, *68*, 849−864.
(18) Caglioti, L.; Hajdu, C.; Holczknecht, O.; Zékány, L.; Zucchi, C.; Micskei, K.; Pályi, G. *Viva Origino* **2006**, *34*, 62.
(19) Buhse, T. *Tetrahedron: Asymmetry* **2003**, *14*, 1055.
(20) Islas, J. R.; Lavabre, D.; Grevy, J.-M.; Lamoneda, R. H.; Cabrera, H. R.; Micheau, J.-C.; Buhse, T. *Proc. Natl. Acad. Sci. U.S.A.* **2005**, *102*, 13743.
(21) Blackmond, D. G. *Tetrahedron: Asymmetry* **2006**, *17*, 584.
(22) Islas, J. R.; Buhse, T. *J. Mex. Chem. Soc.* **2007**, *51*, 117.
(23) Ribo, J. M.; Hochberg, D. *Phys. Lett. A* **2008**, *373*, 111−122.
(24) Crusats, J.; Hochberg, D.; Moyano, A.; Ribo, J. M. *Chem. Phys. Chem* **2009**, *10*, 2123−2131..
(25) Micheau, J.-C.; Cruz, J.-M.; Coudret, C.; Buhse, T. *Chem. Phys. Chem* **2010**, *11*, 3417−3419.
(26) Blackmond, D. G. *Tetrahedron: Asymmetry* **2010**, *21*, 1630−1634.
(27) Doka, E.; Lente, G. *J. Am. Chem. Soc.* **2011**, *133*, 17878−17881.
(28) Gridnev, I. D. *Chem. Lett.* **2006**, 148−153.
(29) Gehring, T.; Busch, M.; Schlageter, M.; Weingand, D. *Chirality* **2010**, *22*, 173−182.
(30) Gridnev, I. D.; Serafimov, J. M.; Brown, J. M. *Angew. Chem., Int. Ed.* **2004**, *43*, 4884−4487.
(31) Klankermayer, J.; Gridnev, I. D.; Brown, J. M. *Chem. Commun.* **2007**, 3151−3153.
(32) Brown, J. M.; Gridnev, I. D.; Klankermayer, J. *Top. Curr. Chem.* **2008**, *284*, 35−65.
(33) Quaranta, M.; Gehring, T.; Odell, B.; Brown, J. M.; Blackmond, D. G. *J. Am. Chem. Soc.* **2010**, *132*, 15104−15107.
(34) Blackmond, D. G.; McMillan, C. R.; Ramdeehul, S.; Schorm, A.; Brown, J. M. *J. Am. Chem. Soc.* **2001**, *123*, 10103−10105.
(35) Buono, F. G.; Blackmond, D. G. *J. Am. Chem. Soc.* **2003**, *125*, 8978−8979.
(36) Buono, F. G.; Iwamura, H.; Blackmond, D. G. *Angew. Chem., Int. Ed.* **2004**, *43*, 2099−2103.
(37) Gridnev, I. D.; Brown, J. M. *Proc. Natl. Acad. Sci. U. S. A.* **2004**, *101*, 5727−5731.
(38) Schiaffino, L.; Ercolani, G. *Angew. Chem., Int. Ed.* **2008**, *47*, 6832−6835.
(39) Schiaffino, L.; Ercolani, G. *ChemPhysChem.* **2009**, *10*, 2508−2515.
(40) Schiaffino, L.; Ercolani, G. *Chem.—Eur. J.* **2010**, *16*, 3147−3156.
(41) Ercolani, G.; Schiaffino, L. *J. Org. Chem.* **2011**, *76*, 2619−2626.
(42) Gridnev, I. D.; A. K. Vorob'ev, Raskatov, E. A. Role of Oligomerization in Soai Reaction: Structures, Energies, Possible Reactivity. In *The Soai Reaction and Related Topic*; G. Pályi, Zucchi, C., Caglioti, L., Eds.; Artestampa: Modena, Italy, 2012; pp 79−122.
(43) Shibata, T.; Yonekubo, S.; Soai, K. *Angew. Chem., Int. Ed.* **1999**, *38*, 59−661.
(44) Busch, M.; Schlageter, M.; Weingand, D.; Gehring, T. *Chem.—Eur. J.* **2009**, *15*, 8251−8258.
(45) By line shape analysis of the signals of pyrimidinyl protons from homo- and heterochiral **2** as it was described in ref 31 for another catalyst. Reich., H. J. *WINDNMR, Line shape analysis software*; 2005.
(46) Dennis, J. E.; Gay, D. M.; Welsch, R. E. *IEEE/ACM Trans. Math. Software* **1981**, *7*, 348−383.

(47) Chang, C. E.; Chen, W.; Gilson, M. K. *J. Chem. Theory Comput.* **2005**, *1*, 1017.
(48) Carlsson, J.; Aqvist, J. *J. Phys. Chem. B* **2005**, *109*, 6448.
(49) Singh, N.; Warshel, A. *J. Phys. Chem. B* **2009**, *113*, 7372.
(50) Becke, A. D. *J. Chem. Phys.* **1993**, *98*, 1372.
(51) Becke, A. D. *J. Chem. Phys.* **1993**, *98*, 5648.
(52) Lee, C.; Yang, W.; Parr, R. G. *Phys. Rev. B* **1988**, *37*, 785.
(53) Zhao, Y.; Truhlar, D. G. *Acc. Chem. Res.* **2008**, *41*, 157.
(54) Frisch, M. J.; Trucks, G. W.; Schlegel, H. B.; Scuseria, G. E.; Robb, M. A.; Cheeseman, J. R.; Scalmani, G.; Barone, V.; Mennucci, B.; Petersson, G. A.; Nakatsuji, H.; Caricato, M.; Li, X.; Hratchian, H. P.; Izmaylov, A. F.; Bloino, J.; Zheng, G.; Sonnenberg, L.; Hada, M.; Ehara, M.; Toyota, K.; Fukuda, R.; Hasegawa, J.; Ishida, M.; Nakajima, T.; Honda, Y.; Kitao, O.; Nakai, H.; Vreven, T.; Montgomery, J. A., Jr.; Peralta, J. E.; Ogliaro, F.; Bearpark, M.; Heyd, J. J.; Brothers, E.; Kudin, K. N.; Staroverov, V. N.; Kobayashi, R.; Normand, J.; Raghavachari, K.; Rendell, A.; Burant, J. C.; Iyengar, S. S.; Tomasi, J.; Cossi, M.; Rega, N.; Millam, J. M.; Klene, M.; Knox, J. E.; Cross, J. B.; Bakken, V.; Adamo, C.; Jaramillo, J.; Gomperts, R.; Stratmann, R. E.; Yazyev, O.; Austin, A. J.; Cammi, R.; Pomelli, C.; Ochterski, J. W.; Martin, R. L.; Morokuma, K.; Zakrzewski, V. G.; Voth, G. A.; Salvador, P.; Dannenberg, J. J.; Dapprich, S.; Daniels, A. D.; Farkas, O.; Foresman, J. B.; Ortiz, J. V.; Cioslowski, J.; Fox, D. J. *Gaussian 09*, Revision A.02; Gaussian, Inc.: Wallingford, CT, 2009.
(55) Ditchfield, R.; Hehre, W. J.; Pople, J. A. *J. Chem. Phys.* **1971**, *54*, 724.
(56) Hehre, W. J.; Ditchfield, R.; Pople, J. A. *J. Chem. Phys.* **1972**, *56*, 2257.
(57) Hariharan, P. C.; Pople, J. A. *Theor. Chim. Acta* **1973**, *28*, 213.
(58) Hariharan, P. C.; Pople, J. A. *Mol. Phys.* **1974**, *27*, 209.
(59) Gordon, M. S. *Chem. Phys. Lett.* **1980**, *76*, 163.
(60) Peng, C. Y.; Schlegel, B. *Isr. J. Chem.* **1994**, *34*, 449.
(61) Barone, V.; Cossi, M. *J. Phys. Chem. A* **1998**, *102*, 1995.
(62) Cossi, M.; Rega, N.; Scalmani, G.; Barone, V. *J. Comput. Chem.* **2003**, *24*, 669.